Thermal Short-Circuit Testing for Large Cross-Sectional Area Components in Modern Power Systems

P. Krasselt[1], M. Bächle[1], R. Badent[1] and T. Leibfried[1]

[1] Institute of Electric Energy Systems and High-Voltage Technology
Karlsruhe Institute of Technology
Engesserstr. 11, 76131 Karlsruhe (Germany)
phone:+49 721 608 43155, e-mail: **Peter.Krasselt@kit.edu**, **Rainer.Badent@kit.edu**, **Thomas.Leibfried@kit.edu**

Abstract. The integration of decentralized renewable energies sources in the electric power system has an impact on electrical components used in transmission and distribution networks. In general, components with high ampacity and large cross-sectional areas are introduced for network connection of large renewable power plants. These components require electrical type testing according to IEC standards. In this paper, a real-time control method for thermal short-circuit testing is proposed. It features automated short-circuit current duration regulation to meet conductor target temperature, which is robust against the phenomena of nonlinear resistance increase due to conductor heating and network voltage sags. Inrush currents are reduced using a phase-lock loop for optimal switch-on time synchronization. For user convenience, the solution features additional automated reporting. Experimental test data on a test stand with an ampacity up to 40 kA validates the concept.

Key words: Power system faults, thermal short-circuit currents, wind energy integration, high-current testing, IEC standards.

1. Medium voltage components: Trend to large cross-sectional areas

Over the last 15 years, a renewable production capacity exceeding 90 GW (2014) has been installed in Germany. Outnumbering the connected thermal power plant capacity of 94 GW (2013) in the next years, the installation of decentralized renewable electricity generation also defines new requirements concerning components for electrical transmission and distribution networks.

To illustrate this point, we will have a closer look on network connections of wind power stations. The publicly available information of installed renewable electricity generation [1] funded under the German Renewable Energy Act is evaluated for the network connection level of each wind turbine generator system. The evaluation shown in TABLE I reveals that nearly half of the installed wind energy capacity is connected to medium voltage (MV) networks.

In the time before the massive integration of renewable electricity generation, standardized conductor sizes up to a cross-sectional area of 300 mm² were sufficient for nearly all challenges in MV network planning. Nowadays, wind farm network connections require a high ampacity, demanding MV products with cross-sectional areas of 500 mm² and more [2,3].

TABLE I. - Wind power stations: network voltage

NETWORK VOLTAGE	CAPACITY	SHARE
Extra high voltage network (EHV)	1.35 GW	4.0 %
Network coupler (EHV-HV)	0.16 GW	0.5 %
High voltage network (HV)	10.95 GW	32.7 %
Network transformer (HV-MV)	5.03 GW	15.0 %
Medium voltage network (MV)	15.85 GW	47.4 %
Distribution transformer (MV-LV)	0.08 GW	0.3 %
Low voltage network (LV)	0.04 GW	0.1 %

2. Thermal short-circuit testing

Electric components are subjected to a variety of electrical, mechanical and thermal stresses. Complex test sequences are defined in product standards to replicate these stresses, and new component designs are type tested according to the relevant standards to ensure safe operation and a long operational life.

Thermal stresses are caused by the Joule effect given in (1): due to the flow of an electric current I for the time t through the conductor with resistance R, a proportional amount of heat Q is generated.

$$Q \sim I^2 \cdot R \cdot t \tag{1}$$

During undisturbed network operation, conductor temperature varies slowly depending on its actual current and ambient conditions. In contrast, conductor temperature rises extremely fast during short-circuits until the fault current is interrupted by power system protection. An adiabatic heating without heat dissipation to the environment can be assumed, reaching conductor temperatures up to 250 °C during the fault current interruption time, which is in the range up to several seconds.

Testing the thermal short-circuit withstand capability of new designed components is therefore an important test procedure. All components directly exposed to the short-circuit current are subjected to this test, e.g. connectors and lugs [4]. Thermal short-circuit testing is also obligatory for accessories (e.g. terminations, straight or branch joints) [5], as their insulation system is stressed by high conductor temperatures after short-circuits.

The method for thermal short-circuit testing is standardized [6]. The test objects are at ambient temperature and are then heated to maximum permissible temperature during short-circuit. For cross-linked polyethylene (XLPE) insulation systems, which dominate the MV market, a target temperature of 250 °C has to be reached within a maximum time of 5 s.
Special attention is required to attain the target temperature as accurately as possible. A direct measurement of TOs temperature using thermocouple elements is very difficult and uncertain due to electro-magnetic disturbance emitted by the short-circuit current.
Therefore, the amount of heat to reach target temperature is theoretically calculated [7], assuming a linear increase of resistance due to heating.

3. Synthetic high-current test circuit

The synthetic high-current test circuit consists of the test object, which is connected to a high-current transformer. To control the 2 MVA high-current transformer, a 20 kV circuit breaker on its MV side is used. For evaluation, the current in the test object is measured by a current probe. The structure of the test setup is shown in Fig. 1.

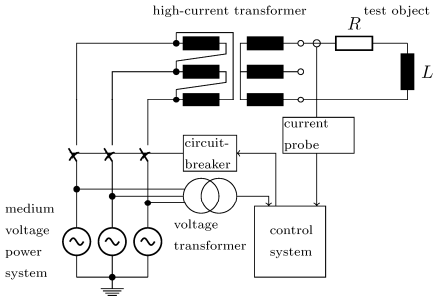

Fig. 1. High-current test setup

A. Conventional approach: open loop time control

In the conventional approach, the initial current is measured with a short-time short-circuit. Assuming a linear increase of resistance due to heating, the full time to reach the target temperature is calculated. Once the test object reached ambient temperature again, a time-controlled short-circuit is applied to the test object with the calculated duration.
This method suffers from the drawback that network voltage variation and voltage sags during high-current testing are neglected. In addition, the short-circuit current amplitude decreases due to resistance increase with higher conductor temperature (TABLE II). This effect reduces networks voltage sag, resulting in a nonlinear dependency between current amplitude and conductor temperature, which degrades the accuracy of the open loop time control.

TABLE II. - Typical increase in resistance

MATERIAL	CONDUCTIVITY / (Ω/m)		INCREASE / (%)
	20 °C	250 °C	
Aluminium	2.82×10−8	5.44×10−8	+92,7
Copper	1.68×10−8	3.20×10−8	+90,4

B. Proposed closed loop approach

Testing products with increasing cross-sectional areas requires more powerful test equipment for thermal testing as the test current varies more nonlinearly. Computational power and analog-digital-converter performance currently available enable a regulation of the required heating time in real-time by an online evaluation of the short-circuit currents.
In this paper, a new real-time control concept for thermal short-circuit withstand tests according to the test methods defined in [6] is introduced. To achieve the required temperature of the test object with high accuracy, a closed loop control is proposed, using a current measurement as a feedback variable.
For optimized operation of the high-current test circuit and minimized MV network disturbance, the elements of the high-current test setup are analyzed in the following.

C. Properties of the high-current test setup

1) *High-current transformer.* For test objects with high cross-sectional area, the impedance is nearly purely inductive. To minimize inrush currents, a phase synchronous switch-on command at the voltage minimum or maximum is preferable to reduce inrush currents of the connected circuit. The transient inrush current of this magnitude will cause a short network voltage sag on the MV side. Furthermore the remanent magnetization of the transformer core has to be considered. Fig. 2 shows the hysteresis diagram of a typical transformer core.
When a remanence has been build-up as a side-effect by the previous test cycle, a current of same polarity as the remanence may lead to saturation effects and an excessively high inrush current, too. As it is practically impossible to measure the residual magnetism, the control system has to estimate it using the recorded waveform of the electrical current of the previous test cycle.
2) *Test Object (TO).* Usually multiple test loops of the TO are subject to testing. As shown in Fig. 1, the TO is modelled by a resistance and an inductance. The resistance is determined by the conductor material, in most cases copper or aluminum, and its temperature.

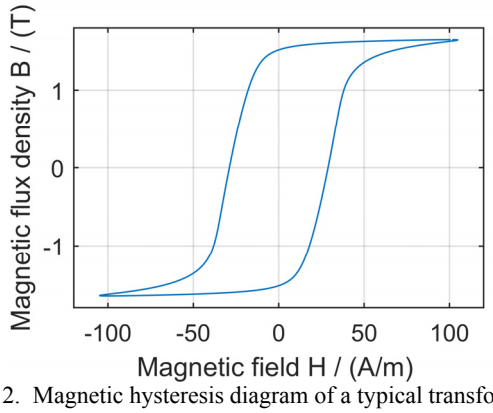

Fig. 2. Magnetic hysteresis diagram of a typical transformer magnetic core

During the thermal short-circuit test, temperature increases significantly, nearly doubling the resistance (TABLE II). The inductance of the test object is defined by the test objects geometric volume and the mounting of the test loop. During testing it does not change.

3) *Circuit-breaker.* A 3-phase circuit-breaker is utilized to switch the high-current transformer on or off. It is important to cope with the switch-on and switch-off delays between the electrical control signal and the switching operation of the circuit breaker. The switch-off delay requires the control system to predict the current during the dead time. These delay times are not constant. A statistical investigation has been performed (Fig. 3). It shows that the standard deviation is small compared to the mean value of the delays (TABLE III). The switch-off variations are inherently greater than the switch-on standard deviation, because a circuit-breaker under load current could only switch-off during the zero crossing of the electrical current.

D. Requirements specification for the control system

Knowing the properties of each part of the high-current test circuit, the control unit has to fulfill the following requirements.

- The discrete joule integral shall be calculated in real-time based on the current waveform.
- For the purpose of data analysis the factual time of open circuit transition shall be determined and recorded.

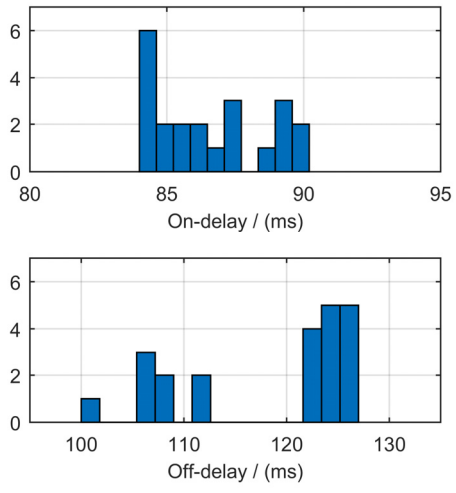

Fig. 3. Distribution of the on- and off-delays of the 3-phase circuit breaker

TABLE III. - Circuit-breaker delay time: statistical distribution

PARAMETER	ON-DELAY	OFF-DELAY
Mean	86.54 ms	118.14 ms
Standard deviation	2.15 ms	8.72 ms

- Due to the switch-off delay of the circuit breaker, an extrapolation of the joule integral shall be used to estimate the particular instant of time at which the switch-off control command must be issued to the circuit breaker.
- To determine the optimum switch-on time, a phase synchronous control has to be implemented.
- To determine the optimum switch-on time, the remanence of the high-current transformer core shall be estimated and the result be taken as set point for synchronized switch-on command.
- For the purpose of user convenience, a unique report displaying all relevant thermal short-circuit parameters shall be generated automatically for each test cycle.

4. Control unit concept

A. Time-discrete calculation of the joule integral

The electrical heating of a current carrying conductor is proportional to the applied joule integral. The joule integral is a time-dependent function:

$$J = \int_{t_0}^{t} i^2(\tau)\, d\tau \qquad (2)$$

The heating of the TO is controlled by calculating the required Joule integral. It is defined in IEC standard 60986 [7] for aluminium conductors according to (3), using copper conductors (4) has to be evaluated.

$$\int_0^t i^2(\tau)\, d\tau = 2.19 \cdot 10^4 \cdot S^2 \cdot \ln\left(\frac{\theta_{sc} + 228}{\theta_i + 228}\right) \qquad (3)$$

$$\int_0^t i^2(\tau)\, d\tau = 5.11 \cdot 10^4 \cdot S^2 \cdot \ln\left(\frac{\theta_{sc} + 234.5}{\theta_i + 234.5}\right) \qquad (4)$$

S is the cross-sectional area of the conductor in mm²
Θ_{sc} is the desired end temperature in °C
Θ_i is the measured start temperature in °C
t is the duration in s

For implementation in a time-discrete control platform, a numerical integration method for determination of the joule integral in (2) has to be selected. The accuracy of the numerical method depends on the spacing of the time steps and the method of numerical integration.
Basing on the sample rate of 100 kS/s of the analog-digital-converter utilized in the control system, a comparison of different numerical integration methods [8] has been performed for a representative current waveform. The referenced current waveform is analytically defined by the following formula:

$$i(t) = 40kA \cdot e^{-\frac{t}{0.04s}} + 30kA \cdot \sin(2\pi \cdot 50Hz \cdot t) \qquad (5)$$

In TABLE IV the results of the exact analytical solution and different numerical integration methods is presented.

TABLE IV. - Comparison of integration methods

INTEGRATION METHOD	JOULE INTEGRAL / ((kA)²s)	RELATIVE DIFFERENCE / (ppm)
Analytical (exact)	939.5913	–
Rectangle rule	939.5990	8.12
Trapezoidal rule	939.5910	-0.39
Simpson´s rule	939.5910	-0.39
Simpson´s 3/8 rule	939.5910	-0.39

For the current waveform given in (5) the joule integral is computed for a duration of 2 s, starting at 0 s. With a more than sufficient accuracy and featuring low computational efforts, the rectangle rule is selected for implementation.

B. Prediction of open circuit transition

The switch-off delay, caused by the circuit-breaker, makes a joule integral prediction necessary. Fig. 4 shows the proposed method based on a linear extrapolation over time using (6).

$$J_{t+t_t} := \int_{t_0}^{t} i^2(\tau)\,d\tau + \frac{t_t}{t_d}\cdot\left(\int_{t_0}^{t} i^2(\tau)\,d\tau - \int_{t_0}^{t-t_d} i^2(\tau)\,d\tau\right) \quad (6)$$

This method assumes a constant root-mean-square (rms) value of the load current during the delay time of the system. However, the joule integral is an integration of square of a sinusoidal function which results in the sum of a monotonically increasing straight line and a superimposed ripple (Fig. 5). The frequency of the ripple is the double of the grid frequency, thus 100 Hz. If the slew rate is calculated using an even integer multiple of the reciprocal value (10 ms), the effects of the ripple will be minimized.
Fig. 5 reveals this in records of actual measurements. Using even larger integration intervals, the prediction will become less vulnerable by noise, but firstly it will be available at a later instant and secondly, it will react to changes of current amplitude with a larger delay. Several integration intervals have been tested. To demonstrate

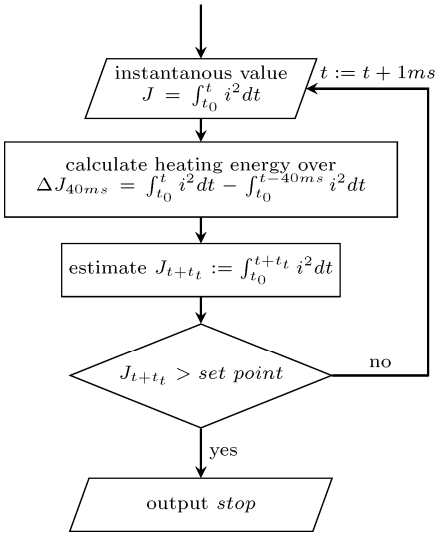

Fig. 4. Algorithm, joule integral prediction

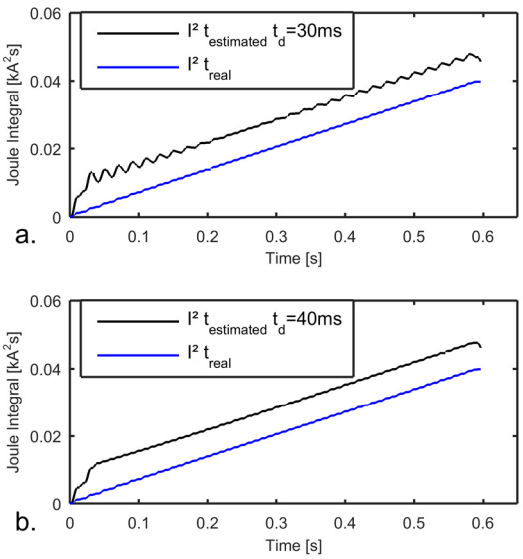

Fig. 5. Joule integral prediction with different slew rate calculations

the influence of the parameter on the quality of the estimation results, Fig. 5 shows two different parameters. An interval of 30 ms promises minimal dead time, but the attenuation of the ripple is not sufficiently achieved. Therefore, an interval of 40 ms has been selected.

C. Identification of closed circuit transition

The control system estimates online the joule integral. Therefore, it is important to detect the correct start time t^* of the short-circuit test. The measured current signals are monitored, and if the signal exceeds a threshold with respect to interfering electromagnetic noise, the current time is set as start time t^* (Fig. 6).

D. Identification of open circuit transition

To identify the particular instant of time when the short-circuit current is interrupted, the method as depicted

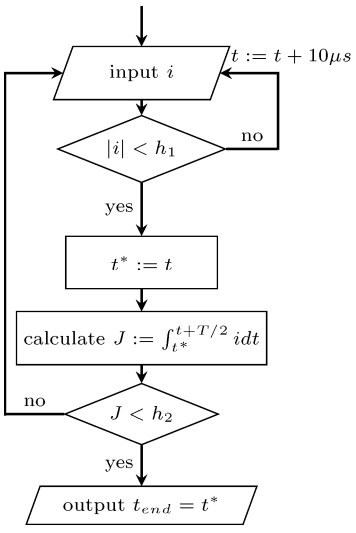

Fig. 6. Algorithm, current termination detection

in Fig. 6 is proposed. It utilizes the insight that high currents can only be interrupted at zero crossings. A natural approach would be to find a zero crossing. As there is high electromagnetic interference in the measurement during current interruption due to arc quenching, an additional criterion is used.
The joule integral over the last detected current half wave is calculated and compared to a threshold. If the calculated value is below the threshold, the end time t_{end} of the test is stored.
The procedure will be repeated until an open circuit transition is recognized. Using the joule integral as additional criterion has the advantage that high frequency noise is attenuated, which makes the algorithm robust.

E. Phase locked loop for grid synchronous trigger

For grid synchronous triggering a phase locked loop has been implemented using a synchronous reference frame phase locked loop (PLL) [9]. As only one phase voltage measurement is available and the PLL algorithm requires a three-phase voltage measurement, a virtual 3-phase system is created using a second order generalized integration as proposed by Cioboaru et al. [10] (Fig. 7).

F. Determining the optimal phase to switch

For inductive loads optimal voltage phases are φ = 90° and φ = 270°. Depending on the remanence of the transformer either 90° or 270° are chosen. The remanence can be calculated by investigating the recorded last half-wave of the previous thermal short-circuit test. If the current was positive in the last half-wave, the transformer should be switched-on at φ = 270° with respect to magnetic saturation.

G. Automated report generation

The automated report generation starts every time when a test cycle has been completed. All the acquired data stored temporarily on the control platform has to be saved to a unique log file located on a computer at the operator test stand.
Essential figures such as the maximum and the effective values of the short-circuit current and the duration of the short-circuit are computed, and visualized on a graphical user interface.
A unique report with the measured data, the calculated characteristic values and the general test setup information is stored as PDF and printed out. The flowchart for the report generation is shown in Fig. 8.

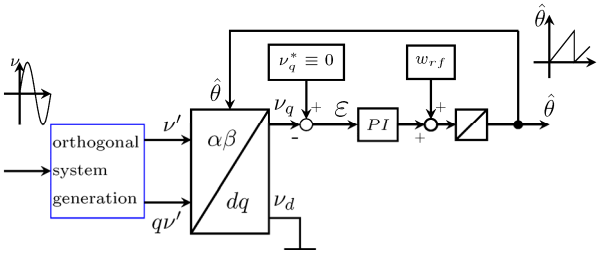

Fig. 7. Single-phase system phase locked loop (PLL) [12]

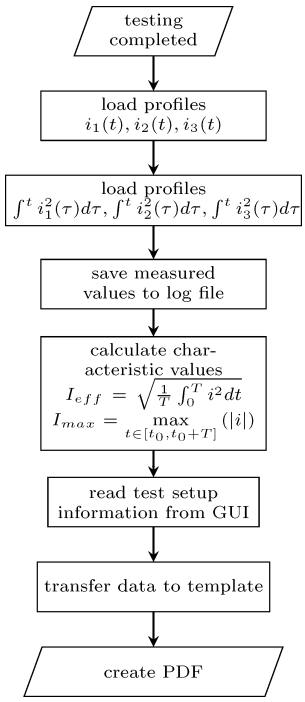

Fig. 8. Flowchart automated report generation

5. Experimental results

A. *Hardware set-up and implementation*

The concept introduced in section 3 has been implemented on a rapid prototyping platform NI compactRIO9076. For analogue data acquisition, a NI9215 module is used with a sample rate of 100 kS/s and a resolution of 16 bit. The short-circuit breaker is controlled by a NI9481 relay module. The high current transformer has a rating of 2 MVA and is capable of short-circuit currents up to 40 kA. The current is measured by Rogowski coil current-probe of type PEM CWT60B for currents up to 12 kA and CWB 600B for currents up to 120 kA. The output signal of the current probe is connected to the analog-digital converter.
The controller includes a real-time processor and a reconfigurable FPGA. The communication with the controller is made through a LAN between a host PC and the real-time operating system on the embedded controller. All the real-time calculations and the controlling operations of the high-current test circuit is implemented in the FPGA.
The thermal short-circuit test cycle can be configured and started through a graphical user interface run on the host PC. In Fig. 9 the signal flow chart of the whole system is shown. For reasons of storing the data in log files and using DIADEM as PDF-creator the automated report generation is done by the host PC.

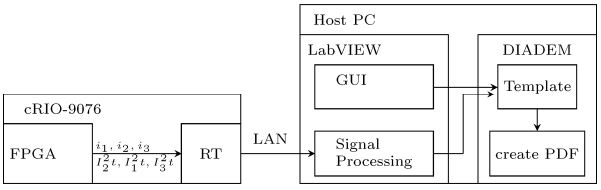

Fig. 9. Signal flow chart of the system

TABLE V. - Joule integral accuracy

PARAMETER	DIFFERENCE / (%)
Average	0.20
Standard deviation	1.96

B. *Determination of control system performance*

For first functional checks of the control unit, an air coil with an inductance of 2 mH has been connected as test object. The high-current transformer is configured to a secondary voltage of 173 V.

To determine the joule integral accuracy, 26 measurements with different joule integral set points have been executed. TABLE V shows the statistical characteristics of the differences to the set point.

Fig. 10 shows exemplary the test object current and the joule integral estimated by the real-time controller. The set point was 0.04 kA²s. When the predicted joule integral is reached at approx. 460 ms, the switch off command is issued (section 3.2) to the circuit-breaker.

Fig. 11 shows the different behavior of the current when using different phase angles to switch-on the transformer. An optimal switch-on phase of φ = 90° is recorded in the upper graph. For comparison, a short-circuit test with a switch-on phase of φ = 0° has been recorded in the lower graph of Fig. 11. An excessively large inrush current superimposes the steady-state short-circuit current.

In Fig. 12 the influence of the remanence is shown. Phase angle was set in both test to the same value of φ = 90°. The only difference is that in the upper diagram, the transformer had a positive remanence and in the lower diagram the remanence was negative.

With correct phase setting, no voltage sag in the recorded network voltage is observed, and the TO voltage is sinusoidal. With incorrect phase setting, a network voltage sag of 6.5 % occurs and the voltage on the TO harmonic distortion due to magnetic core saturation.

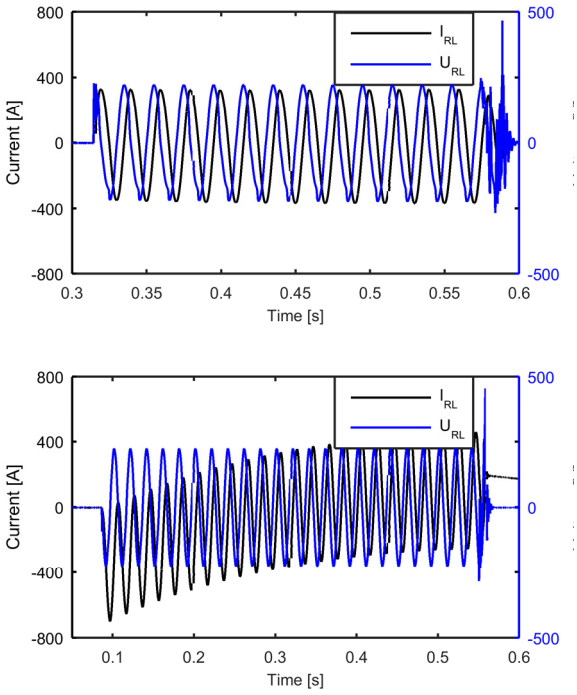

Fig. 11. Measurement air coil φ = 90°, φ = 0°

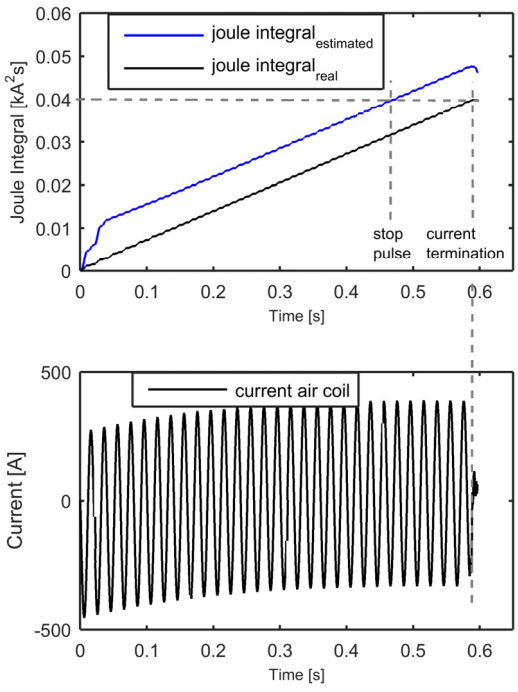

Fig. 10. Exemplary short-circuit test data

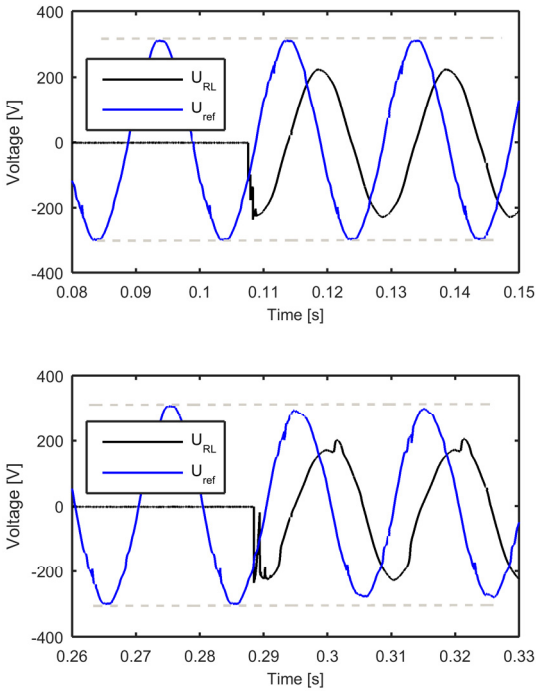

Fig. 12. Experimental test of influence of transformer remanence

C. *Thermal short-circuit testing*

For final commissioning, a 1,000 mm² copper rail has been connected as test object to the high-current transformer, which is configured for a secondary voltage of 70 V. With an calculated resistance of 6.1 µΩ and an inductance of 6.5 µH, a steady stead current of approx. 20 kA is expected. The control unit is configured to a joule integral setpoint of 300.0 (kA)²s.
Fig. 13 shows the recorded values, and the evaluated parameters of the test are given in TABLE VI. As it can be seen, the control unit performs the high-current tests with a high accuracy.
Finally in Fig. 14 an automatically generated report is reproduced. As TO a 300 mm² aluminium conductor was used. The temperature set point was 255 °C. To reach this end temperature, a joule integral set point of 1313 (kA)²s was calculated using equation (3.2). A joule integral of 1316 (kA)²s has been achieved, resulting in an end temperature of 255.5 °C.

TABLE VI. - Results of 1,000 mm² copper rail measurement

PARAMETER	VALUE
Secondary voltage	70 V
I²t set point	300.0 (kA)²s
I²t achieved	303.0 (kA)²s
Ipeak	38.6 kA
Irms	22.7 kA
Duration t	588.3 ms

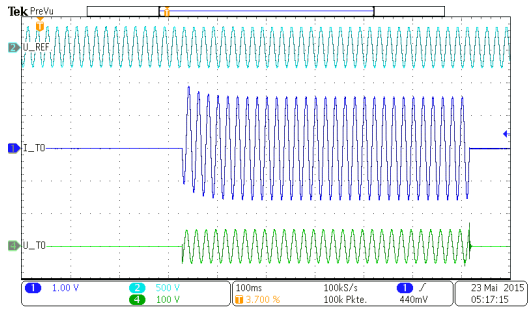

Fig. 13. Oscillogram of final commissioning
CH1: Test object current, 20 kA/div (blue)
CH2: Reference network voltage, 500 V/div (cyan)
CH4: Test object voltage, 100 V/div (green)
Time scale: 100 ms/div

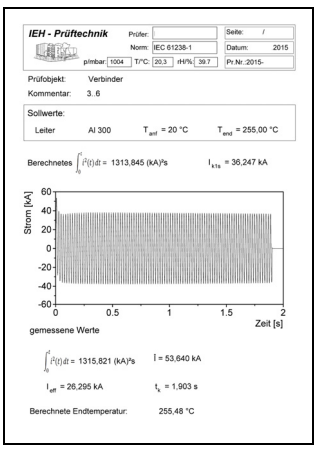

Fig. 14. Example of an automatically generated report, test object: 300 mm² aluminium connector

5. Conclusion

Conductors with high cross-sectional areas are nowadays widely introduced for network connection of renewable electricity generation. These components are subjected to standardized testing [6]. Increasing cross-sectional areas require higher rated and more accurate controlled thermal short-circuit tests stands.
A real-time control of the short-circuit current duration is proposed in this paper. By determining the specific energy the test object is subjected to, it effectively deals with nonlinear decreasing test currents. Dead times for short-circuit interruption are considered using a prediction of the measured current values. In addition, the control system features a phase locked loop for network voltage synchronization, allowing an optimized switch-on phase for minimized network disturbance during testing. For convenience, the control systems assists the test stand operator with an automated evaluation of each thermal short-circuit.
The control concept has been implemented on a rapid prototyping solution and used for experimental testing on a high-current transformer. The results prove reliable operation of the test system and a high accuracy of the control solution, fulfilling standardized requirements.

References

[1] Network transparency internet information platform of the German transmission system operators, http://www.netztransparenz.de, last accessed 2015-06-10.
[2] Z. Chen, “Issues of Connecting Wind Farms into Power Systems”, in *Proc. of the 2005 IEEE/PES Transmission and Distribution Conference & Exhibition: Asia and Pacific*, Vol. 1, pp. 1-6, Dalian, China, 2005.
[3] German association of energy and water industries (BDEW), “Technical Guideline: Generating Plants Connected to the Medium-Voltage Network”, 2008.
[4] IEC international standard 61238-1:2003, “Compression and mechanical connectors for power cables for rated voltages up to 30 kV (Um = 36 kV)”, 2003.
[5] IEC international standard 60502-4:2010, “Power cables with extruded insulation and their accessories for rated voltages from 1 kV (Um = 1,2 kV) up to 30 kV (Um = 36 kV) - Part 4: Test requirements on accessories for cables with rated voltages from 6 kV (Um = 7,2 kV) up to 30 kV (Um = 36 kV)”, 2010.
[6] IEC international standard 61442:2005, “Test methods for accessories for power cables with rated voltages from 6 kV (U_m = 7,2 kV) up to 30 kV (U_m = 36 kV)”, 2005.
[7] IEC international standard 60986:2000, “Short-circuit temperature limits of electric cables with rated voltages from 6 kV (Um = 7,2 kV) up to 30 kV (Um = 36 kV)”, 2000.
[8] A.R. Krommer and C.W. Ueberhuber, “Numerical Integration: on Advanced Computer Systems”, Springer, Berlin Heidelberg, 1994
[9] L.N Arruda, S.M. Silva and B.J.C Filho, “PLL structures for utility connected systems,” *Conference Record of the 2001 IEEE Industry Applications Conference*, Vol. 4, pp. 2655-2660, Chicago, USA, 2001.
[10] M. Ciobotaru, R. Teodorescu, and F. Blaabjerg, “A New Single-Phase PLL Structure Based on Second Order Generalized Integrator”, in *Proc. of the 37th IEEE Power Electronics Specialists Conference (PESC ’06)*, pp. 1-6, Orlando, USA, 2006.